Gamow-Teller strength in ^{60,62,64}Ni(n,p) reactions at 198 MeV

A. L. Williams,[1,*] W. P. Alford,[2] E. Brash,[3,†] B. A. Brown,[4] S. Burzynski,[3,‡] H. T. Fortune,[1] O. Häusser,[3,5] R. Helmer,[5] R. Henderson,[5] P. P. Hui,[1] K. P. Jackson,[5] B. Larson,[3] M. G. McKinzie,[1] D. A. Smith,[1] A. Trudel,[3,5] and M. Vetterli[5]

[1] *University of Pennsylvania, Philadelphia, Pennsylvania 19104*
[2] *University of Western Ontario, London, Ontario, Canada N6A 3K7*
[3] *Simon Fraser University, Burnaby, British Columbia, Canada V5A 1S6*
[4] *Michigan State University, East Lansing, Michigan 48824*
[5] *TRIUMF, 4004 Wesbrook Mall, Vancouver, British Columbia, Canada V6T 2A3*

(Received 31 October 1994)

Measurements of the (n,p) reaction cross section on ^{60,62,64}Ni have been made at 198 MeV for $\theta_{\rm lab}$=0–20° in 4° steps. Multipole analyses have been performed on the resulting spectra and Gamow-Teller (GT) strength distributions have been obtained. These GT distributions have been found to occur as strong peaks at low excitation energy in the final Co nuclei and extend weakly upwards to 30 MeV of excitation. Comparisons of the data with renormalized shell-model calculations show reasonable agreement at low excitation, though the calculations predict very little strength at excitation energies above about 6 MeV.

PACS number(s): 25.40.Kv, 24.30.Cz, 27.50.+e

I. INTRODUCTION

Nucleon charge exchange reactions have provided an important probe of the spin-isospin response of nuclei. For incident energies above ~100 MeV, the isovector spin-flip component of the effective interaction has been shown to be most important [1,2], so that reaction cross sections arise mainly from spin-isospin transitions. In particular, for small momentum transfer, q (forward angles and low excitation energies), Gamow-Teller (GT) transitions, with $\Delta L = 0$, $\Delta S = 1$, $\Delta J^{\pi} = 1^{+}$, will dominate the spectrum, and it has been shown that the $\Delta L = 0$ cross section, extrapolated to $\Delta q = 0$, for (n,p) $[(p,n)]$ reactions is proportional to the β^{+} (β^{-}) decay strength for GT transitions between the same states [1]. In this work, we have measured differential cross sections for the ^{60,62,64}Ni(n,p) reactions at 198 MeV, and have used the results to determine the distribution of GT strength in the final nuclei ^{60,62,64}Co.

Knowledge of the GT strength distributions in fp-shell nuclei is required for model calculations of presupernova stellar collapse [3–6]. In the precollapse stellar core the pressure of the degenerate electron gas provides much of the support for the outer layers of the star. However, as the temperature of the core increases, the electron energies increase until electron capture on core nuclei, mainly via GT transitions, becomes important. Eventually the mass of the core exceeds the Chandrasekar limit, $M_c = 5.8\ Y_e^2 M_s$, where M_s is the solar mass and Y_e the ratio of electrons to nucleons in the core. At that point the core becomes unstable against gravitational collapse, and the ensuing collapse may result in creation of a supernova. Since the core is composed mainly of nuclei in the iron region just before collapse, GT strengths for fp-shell nuclei are required to permit the calculation of electron capture rates on these nuclei [7]. The present measurements provide a direct determination of the distribution of GT strength for the electron capture on the isotopes ^{60,62,64}Ni.

For cases of astrophysical interest which cannot be measured directly, such as unstable nuclei, GT strength distributions must be estimated by model calculations. The present results are also of interest for comparison with model calculations in order to provide a basis for judging the reliability of calculated distributions.

A quantity which is required in determining GT strengths from charge-exchange measurements is the cross section per unit GT strength [1], $\hat{\sigma}_{\rm GT}(E,A)$, which connects measured cross sections with GT transition strengths

$$\hat{\sigma}_{\rm GT}(E,A) = \sigma(q=0)/B_{\rm GT}. \tag{1}$$

For certain cases in which the β-decay strength is known, the unit cross section has been determined experimentally. From these data, the energy and mass dependence of the unit cross section has been obtained as a fit to the expression [8]

$$\hat{\sigma}_{\rm GT}(E,A) = C_1(1 + C_2 e + C_3 e^2)(1 + C_4 A^{1/3} + C_5 A^{2/3}) \tag{2}$$

(where $C_1 = 6.26$ mb/sr, $C_2 = 0.079$ MeV^{-1}, $C_3 = -0.035$ MeV^{-2}, $C_4 = 0.574$, and $C_5 = -0.167$; $e = E$(in

*Present address: Johns Hopkins Oncology Center, Baltimore, MD.

†Present address: Rutgers University, Piscataway, NJ.

‡On leave from Instituite for Nuclear Studies, Swierk, Poland.

MeV)/100.0–1.0). Values of $\hat{\sigma}$ obtained from the reactions ^{6}Li and ^{12}C(n,p) and ^{12}C, ^{18}O, ^{19}F, ^{26}Mg, ^{27}Al, ^{39}K, ^{42}Ca, and ^{54}Fe(p,n) at medium energies were fitted to determine the above coefficients. This expression for $\hat{\sigma}$ is seen to vary slowly with incident energy E, and with atomic number A. Once measured for a nucleus in a given mass region, the unit cross section can be used to extract $B_{\rm GT}$ from cross section measurements for other nuclei of comparable mass. Currently the behavior of $\hat{\sigma}$ for $A \leq 40$ is better determined than for fp-shell nuclei.

The (n,p) reaction on ^{64}Ni presents an opportunity to measure the unit cross section for fp-shell nuclei. The β^- decay of ^{64}Co(g.s.) to ^{64}Ni(g.s.) is the strongest GT transition between nuclear ground states in the fp shell, with log(ft) =4.27±0.02 [9,10]. This is related to the GT strength [1] by

$$B^-_{\rm GT} = \frac{6166 \pm 2 \text{ s}}{(g_A/g_V)^2\, ft} = 0.209 \pm 0.012 \ , \qquad (3)$$

where $(g_A/g_V) = 1.260 \pm 0.008$ from the beta decay of the free neutron [11], for which $B_{\rm GT} = 3$. The value of $B^+_{\rm GT}$ required for comparison with the (n,p) measurements is related to $B^-_{\rm GT}$ by detailed balance [12]

$$B^+_{\rm GT} = \frac{2J_f + 1}{2J_i + 1} B^-_{\rm GT} = 0.627 \pm 0.036 \qquad (4)$$

where J_i and J_f are the spins of initial and final states in the (n,p) reaction.

II. EXPERIMENT

Measurements presented here were made at the TRIUMF charge exchange facility [13] using neutrons produced by the ^{7}Li(p,n) reaction on a target of thickness 110 mg/cm^2. The proton beam of nominal energy 200 MeV was momentum dispersed, and the width of the target was chosen to give a beam energy spread of about 400 keV on target. This reaction produces neutrons with similar intensity for transitions to the ^{7}Be ground state and first excited state at 0.43 MeV. There is also a continuum of neutrons produced up to about 60 MeV in excitation with an intensity of about 1%/MeV of that for the discrete states. Incident proton currents of 500–600 nA were typical, producing a neutron flux of $\sim 10^5$/cm^2 s for 2×5 cm^2 target areas.

Targets were housed in a target box [14] which allows up to six targets to be measured simultaneously, with up to three stacks of six targets in the box at a given time. For a given stack, the six targets are separated by proportional wire chamber planes to allow target identification for each proton event detected. Position and direction information for each proton event is provided by two drift chambers positioned after the target box, and momentum analysis is done with the medium resolution spectrometer (MRS). Spectra were obtained for MRS angles of 0°, 4°, 8°, 12°, 16°, and 20° with angular acceptance ±2°. Mean c.m. scattering angles were measured for each target position in the target box. For the ^{64}Ni target, which was the Ni target furthest downstream, mean c.m. scattering angles were observed to be 1.6°, 4.4°, 8.3°, 12.2°, 16.0°, and 19.9°. Target positions further upstream (^{60,62}Ni) yielded slightly larger mean c.m. scattering angles than for ^{64}Ni, more evident at larger spectrometer angle settings. Proton spectra were recorded up to excitation energies of about 35 MeV. The energy resolution was 750 keV as measured for a CH_2 target in the furthest downstream position F. Due to proton straggling in subsequent targets, the resolution was found to be slightly poorer for the Ni targets, with Γ(FWHM) $\sim$ 930, 860, and 800 keV for the ^{62}Ni, ^{60}Ni, and ^{64}Ni targets, respectively. Target configurations and densities are shown in Table I. The CH_2 target was used to observe protons from the ^{1}H(n,p) reaction. A comparison of the measured count rate with the cross section calculated from nucleon-nucleon phase shifts using the program SAID [15] provided a measurement of incident neutron flux on the target box. The graphite target was used to permit subtraction of the contribution from the ^{12}C(n,p) reaction to the observed spectrum from the CH_2 target. This provided a measurement of the true spectrum of incident neutrons which is required in order to deconvolute the effect of the neutron continuum in the measured spectra. Two other stacks were employed. One contained six CH_2 slabs and was used to check the relative neutron flux and proton detection efficiency vs target position. The other stack consisted of five empty slots with one CH_2 target in position F, which was used to monitor background and also for target box wire chamber efficiency tests.

Spectra obtained with this system must be corrected for background arising mainly from the ^{1}H(n,p) reaction occurring in the cathode planes of the target box chambers plus some contribution from other components. Presented in Fig. 1(a) is a raw spectrum for ^{64}Ni taken at $\theta_{\rm MRS} = 0°$ and in Fig. 1(b) the spectrum after background subtraction. The most obvious change is the

TABLE I. Target stack arrangement and areal densities.

Position[a]	Target	Dimensions (cm^2)	ρ_x (mg/cm^2)	Enrichment (%)
A	$^{\rm nat}$C (graphite)	5.0 × 2.5	147	
B	^{62}Ni (metal foil)	9.5 × 2.5	147.5	96.72
C	^{62}Ni (metal foil)	9.5 × 2.5	147.5	96.72
D	^{60}Ni (metal foil)	7.5 × 5.0	150.5	99.07
E	^{64}Ni (metal foil)	7.5 × 5.0	145.6	97.93
F	CH_2 (polyethylene)	5.0 × 2.5	44.8	

[a]Position A is upstream.

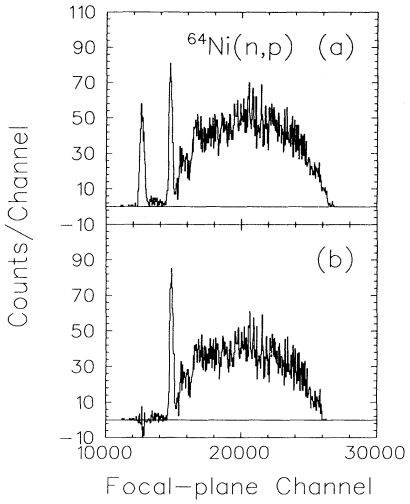

FIG. 1. (a) Raw spectrum for ^{64}Ni(n,p) measured at $\Theta_{c.m.} = 1.6°$; (b) same spectrum after background subtraction.

removal of the peak near channel 13 000 which arises from the ^{1}H(n,p) reaction. After background subtraction, spectra were corrected for spectrometer acceptance, and the incident neutron continuum was deconvoluted from each. The normalized ^{60,62,64}Ni(n,p) spectra were then binned in 300 keV bins and are shown in Figs. 2–4.

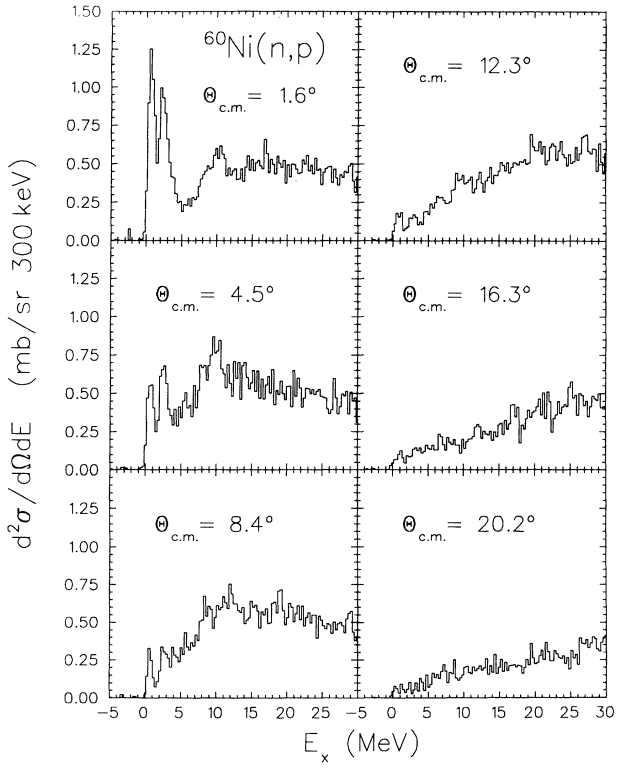

FIG. 2. Binned spectra at the indicated c.m. angles for ^{60}Ni$(n,p)^{60}$Co plotted vs excitation energy. The spectra have been binned in 300 keV steps.

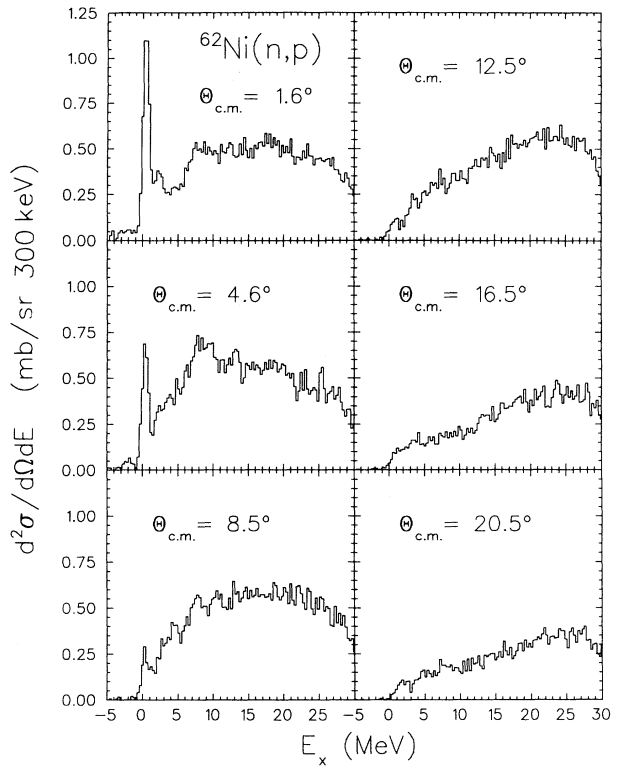

FIG. 3. Binned spectra at the indicated c.m. angles for ^{62}Ni$(n,p)^{62}$Co plotted vs excitation energy. The spectra have been binned in 300 keV steps.

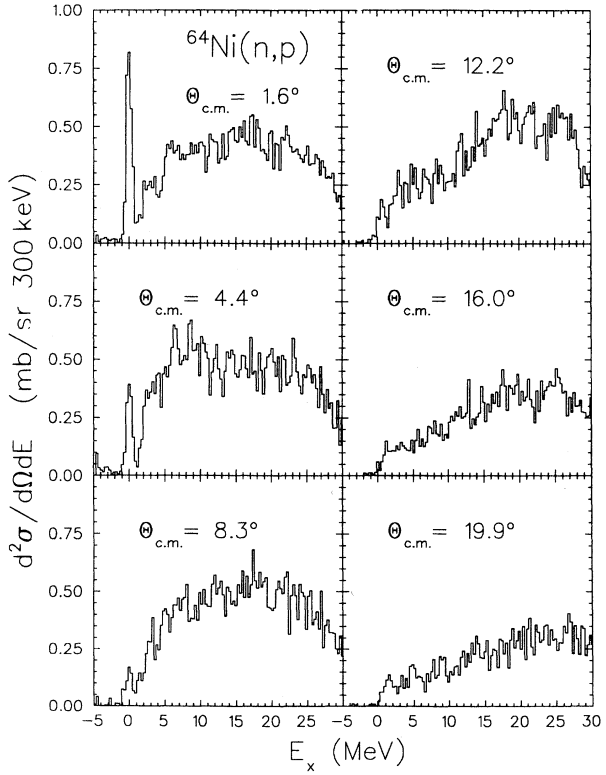

FIG. 4. Binned spectra at the indicated c.m. angles for ^{64}Ni$(n,p)^{64}$Co plotted vs excitation energy. The spectra have been binned in 300 keV steps.

III. RESULTS

A. Unit cross section

For the ^{64}Ni(n,p) reaction we have extracted cross sections (Fig. 5) for the peak near $E_x = 0$ MeV. The forward peaking of the measured cross sections indicates the importance of the GT transition to the $J^\pi = 1^+$ ground state of ^{64}Co. However, with the experimental energy resolution of about 800 keV, the cross sections may include contributions from transitions to excited states as well as the ground state. Measurements of the ^{64}Ni$(t,^3$He$)^{64}$Co reaction [16] identified seven levels below 1 MeV excitation but provided no spin assignments. The β^+ decay of ^{64}Fe [17] populates the ground state of ^{64}Co, plus a state at 0.311 MeV which is identified as a 1^+ state. This state is probably the same as the state observed at 0.296 MeV in the $(t,^3$He) measurements. These results would suggest that the cross sections of Fig. 5 could include a contribution from a GT transition to the 0.311-MeV state.

The experimental resolution precluded the separate determination of peak areas for the ^{64}Co g.s. and 0.311-MeV (1^+) state by a fitting procedure. Instead, the degree of contamination from the excited state was obtained by an analysis of the Q value of the "g.s." peak, which occurs as an isolated structure (Fig. 4). The Q value for the centroid of the peak was determined by comparison of the peak location relative to that for the ^{1}H(n,p) and ^{12}C(n,p) reactions at the MRS angle of 0°.

Accurate determination of a Q value depends on knowledge of incident energy, outgoing energy (momentum), and energy loss in the target(s). Given an absolute momentum calibration of the spectrometer system, positions of the ^{1}H and ^{12}C peaks determine the beam energy and mean scattering angle. Location of the ^{64}Ni peak then determines the ^{64}Ni Q value, after correcting for target energy loss. In this method, exact knowledge of mean scattering angle is not required. Another method works if the relationship between momentum and focal-plane channel number is known to be linear. In that case, the calibration is not needed, because we have three peaks—known ^{1}H, ^{12}C Q values and the unknown ^{64}Ni Q-value lying roughly halfway between the other two. This determination of the unknown Q value is relatively insensitive to the beam energy, but does depend on knowledge of the mean scattering angle, because kinematic shifts are considerably different for the three target nuclei. An uncertainty of 0.1° in mean scattering angle makes a 10 keV change in the ^{64}Ni Q value, and we think that we know the mean scattering angle to at least this accuracy.

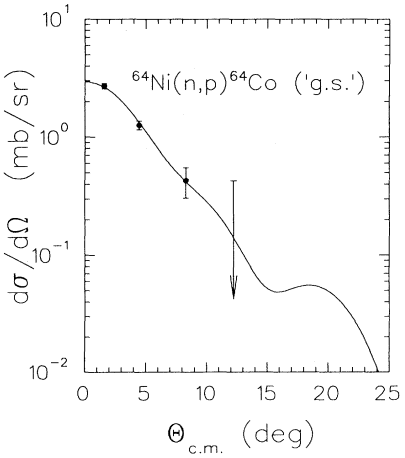

FIG. 5. Differential c.m. cross sections (mb/sr) for the peak near $E_x = 0$ MeV in ^{64}Ni$(n,p)^{64}$Co. The solid line is a DWIA curve normalized to the data as described in the text.

Both methods depend in the same way on target energy losses. In the present case, ^{1}H and ^{12}C are in the same CH_2 target, and (n,p) events correspond to protons having traversed, on average, one-half of the CH_2 target. Protons from events in ^{64}Ni traverse, on average, one-half the ^{64}Ni target, one additional wire chamber plane and all of the CH_2 target. In the actual targets used, our energy-loss calculations give 491 and 225 keV for total thicknesses of ^{64}Ni and CH_2 targets, respectively, and 10 keV for the energy loss in one wire chamber plane. Thus $\Delta E_{\rm loss} = 368$ keV with an estimated uncertainty of 5 keV for ^{64}Ni(n,p) events with respect to (n,p) events occurring within the CH_2 target.

Using a spectrometer focal-plane channel-to-momentum calibration determined for this experiment and measured ^{1}H, ^{12}C, and ^{64}Ni peak locations gives $Q(^{64}\text{Ni}) = -6.662 \pm 0.031$ MeV. The method of linear interpolation results in $Q(^{64}\text{Ni}) = -6.636 \pm 0.031$ MeV. For both methods the same energy loss correction was made, and all uncertainties have been added in quadrature. It is gratifying that the two numbers agree so well. The spectrometer calibration is not linear, but the quadratic term is small. The final value we quote, -6.649 ± 0.031, is the average of the two values above, and we retain the common uncertainty. The most recent estimate of the Q value for the ground-state transition from the known nuclear masses [18] is $Q_{\rm g.s.} = -6.5245 \pm 0.0202$ MeV. The comparison of these Q values implies that the peak includes a contribution from the 0.311-MeV excited state transition which is 40% ± 16% of the "g.s." peak.

The $(t,^3$He) measurement reported a cross section to the 0.296-MeV (0.311-MeV) state to be 27% of the g.s. However, because that experiment was performed at low energy the relevant interpretation is uncertain. In particular, the momentum transfer in the $(t,^3$He) experiment is greater at smaller angles than for this work. The β^- decay strengths of ^{64}Fe are not relevant to the ^{64}Ni$(n,p)^{64}$Co process, and hence do not aid this analysis. Inelastic proton scattering at 200 MeV on ^{58,60,62,64}Ni [19] measured angular distributions to analogs of the parent states which appear as low-lying GT peaks in this (n,p) experiment. The analog of the ^{64}Co g.s. is computed to lie at about 15.68 MeV of excitation in ^{64}Ni. The (p,p') experiment, with superior resolution to this work, identifies a $T_0 + 1$ component of the $M1$ resonance at 15.62 MeV of excitation in ^{64}Ni. A strong state 0.311 MeV above this $M1$ is not observed which would suggest little or no contribution from an excited state to the ^{64}Co g.s. cross section.

In order to calculate $\hat{\sigma}_{GT}$ from measured cross sections it is necessary to extrapolate the cross section back to $q = 0$. This was done using distorted-wave impulse-approximation (DWIA) calculations for a transition of interest. For this work we have used the program DW81 [20] with entrance and exit channel optical potentials generated by folding the Franey and Love interaction [21] with a nuclear matter distribution using MAINX8 [22]. Single-particle states in the transition amplitude were harmonic-oscillator states with oscillator parameter b =1.9 fm, and the transition was assumed to take place between shell-model states $\pi 0f_{7/2} \rightarrow \nu 0f_{5/2}$. These calculations were thus identical to DWIA calculations used in analyses of measurements of (n,p) reactions on other fp-shell nuclei [23–25].

Curves were calculated, one with no energy loss in the reaction, and one with the ^{64}Ni reaction Q value (−6.52 MeV). The latter curve was fitted to the measured cross sections at the two most forward angles. The normalized curve along with the data are shown in Fig. 5. This curve was then used to extrapolate the measured cross sections back to $\theta = 0°$, $\sigma_{exp}(\theta \rightarrow 0)$. This procedure results in $\sigma(0°) = 2.943 \pm 0.131$ mb/sr. A final extrapolation to obtain $\sigma(q = 0)$ has been made as for [1]:

$$\sigma\,(q=0) = \sigma_{\rm exp}\,(\theta \rightarrow 0) \times \frac{\sigma_{\rm DW81}\,(\theta = 0, Q = 0)}{\sigma_{\rm DW81}\left[\theta = 0, Q = Q_{(n,p)}\right]}. \tag{5}$$

The latter factor in Eq. (5) was calculated to be 1.14 so that $\sigma(q = 0) = 3.35 \pm 0.15$ mb/sr. Using B_{GT}^{np} as given in Eq. (4), we get $\hat{\sigma}_{GT} = 5.34 \pm 0.39$ mb/sr. This value of $\hat{\sigma}$ assumes no contribution from an excited state at 0.311 MeV, and is consistent with LAMPF measurements [26] at nearby energies which would also include any excited-state contributions.

A value for $\hat{\sigma}$ which includes the large systematic uncertainty in the excited state contribution from our Q-value analysis would be $\hat{\sigma} = 3.2 \pm 0.9$, where all errors have been added in quadrature.

B. Gamow-Teller strength distributions

At the most forward angle, substantial strength was observed in peaks at low-lying excitation energies for these measurements (see Figs. 2–4)—an indication of GT strength. At higher excitation, as well as larger angles, it is expected that $L > 0$ multipole contributions will be important. In order to estimate GT strength from the results it was necessary to determine these contributions. This was accomplished via a multipole decomposition analysis [27] of the measured spectra using representative angular distributions for each L transfer expected to be important. Following the approach used in analyzing earlier measurements of (n,p) cross sections for fp-shell nuclei [23–25], it was assumed that the data could be satisfactorily represented by a superposition of only four "typical" angular distributions for transitions with $\Delta L = 0$, $\Delta J^\pi = 1^+$; $\Delta L = 1$, $\Delta J^\pi = 1^-$; $\Delta L = 2$, $\Delta J^\pi = 2^+$; $\Delta L = 3$, $\Delta J^\pi = 3^-$. Theoretical shapes were calculated using the DWIA code DW81 assuming single particle transitions $(\pi 0f_{7/2})^{-1}(\nu 0f_{5/2})$ for $\Delta L = 0$, 2, and $(\pi 0f_{7/2})^{-1}(\nu 0g_{9/2})$ for $\Delta L = 1$, 3. Single-particle states and optical potentials were as described in the earlier discussion of unit cross sections.

For the multipole analyses, the raw data were summed in bins of width 1 MeV. For each bin the resulting angular distribution was then fitted to a sum of DWIA shapes for the appropriate excitation energy using a least-squares procedure. The resulting fits are shown in Figs. 6–8 for the three targets studied. The error bars shown in these figures represent the statistical uncertainties in the data only.

It is seen that the fit to the data is generally good, except at the largest spectrometer angle where the predicted cross section is too small. This probably indicates the need for a component with $\Delta L > 3$ in the analysis. In addition, in the fits to the data at $\theta_{MRS} = 4°$, the analysis consistently underpredicts the measured cross section in the vicinity of 8 MeV excitation. A possible explanation for this is that transitions with $\Delta J^\pi = 0^-$, for which the angular distributions are more forward peaked than for $\Delta J^\pi = 1^-$, might be stronger than expected. This is considered unlikely though since RPA calculations for ^{60}Ni [28] predict that the centroid of 0^- strength lies near 16 MeV, above that for 1^- strength. Another possible explanation is that the DWIA calculations for ΔL =1 transitions predict a forward angle cross section that is

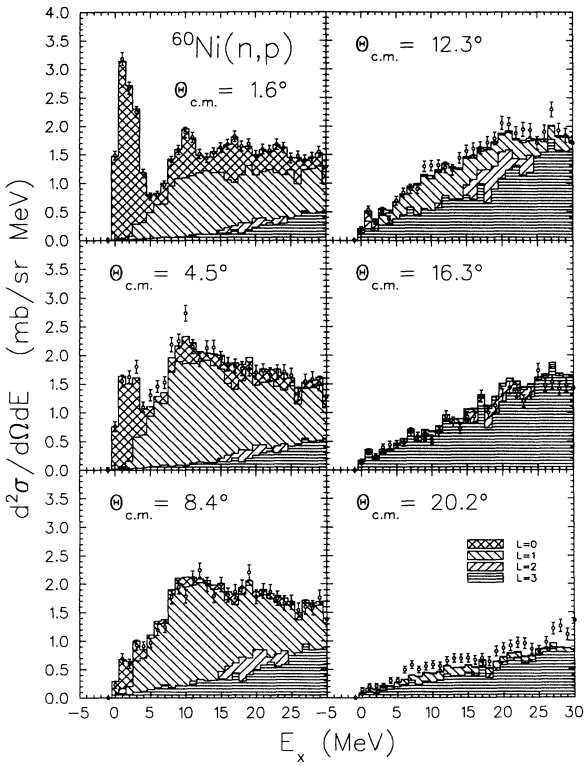

FIG. 6. Results of the multipole decomposition analysis for the ^{60}Ni(n,p) data with multipole contributions shown. Error bars are statistical only.

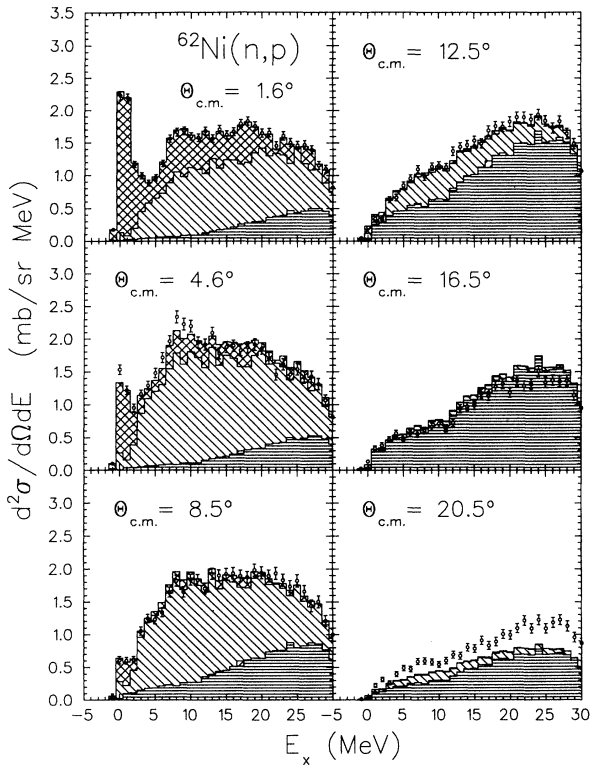

FIG. 7. Results of the multipole decomposition analysis for the ^{62}Ni(n,p) data with multipole contributions shown. Error bars are statistical only.

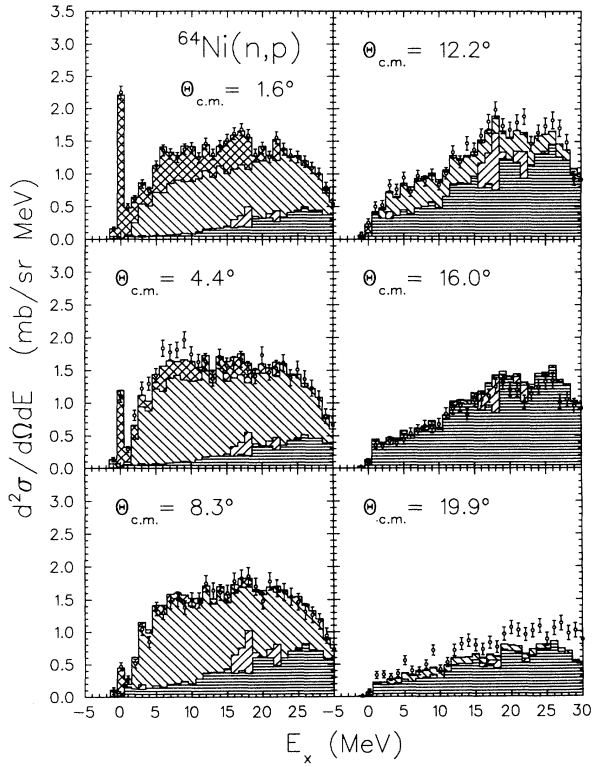

FIG. 8. Results of the multipole decomposition analysis for the ^{64}Ni(n,p) data with multipole contributions shown. Error bars are statistical only.

slightly smaller than the experimental data, as found for a recent (p,n) experiment at 394 MeV on ^{16}O and ^{18}O [29].

The cross section for the ΔL =0 component of the multipole decomposition at 1.6° is shown as a function of excitation energy for each target in Fig. 9. In this figure, the error bars again represent the statistical uncertainty only. At low excitation energies, where the measured angular distributions are strongly peaked in the forward direction, the ΔL =0 component extracted from the analysis is insensitive to the assumed shapes for $\Delta L > 0$, and the error bars provide a reasonable estimate of the overall uncertainty. At higher excitation energies however, above about 8 MeV, the measured angular distributions are not as forward peaked, and the ΔL =0 strength extracted is sensitive to the details of the shape of the DWIA predictions for ΔL =1 transitions at forward angles. Thus the estimate of ΔL =0 cross sections above about 8 MeV excitation is subject to systematic uncertainties which are difficult to specify quantitatively, but which may be quite large.

The analysis indicates the existence of ΔL =0 strength up to high excitation energies, and some would be ex-

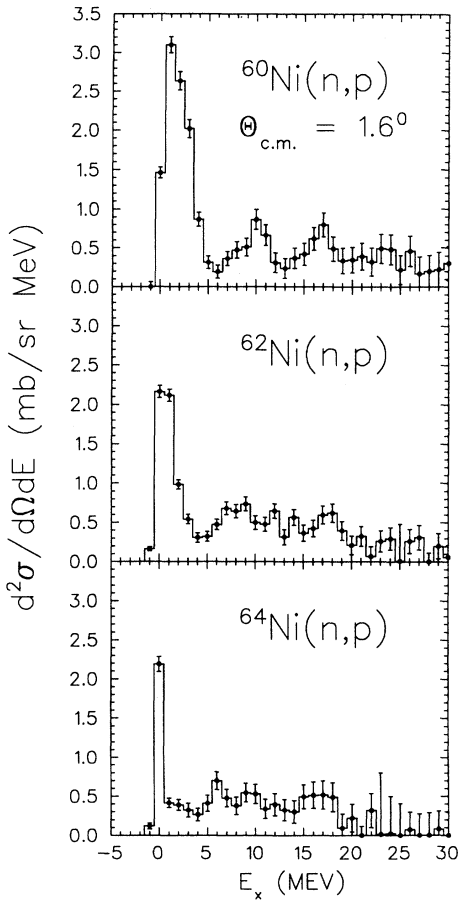

FIG. 9. Excitation-energy dependences of the cross sections at $\Theta_{c.m.}$ = 1.6° for the ΔL =0 components of the reactions shown.

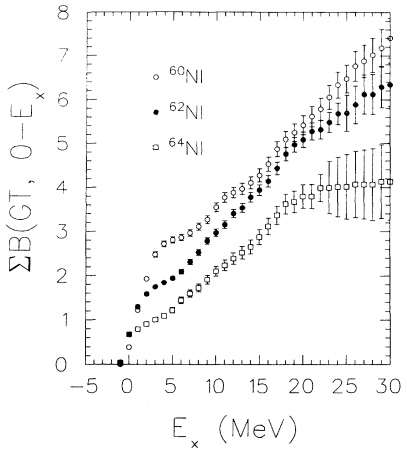

FIG. 10. The experimental running sums $\sum_{Ex=0}^{E} B_{\rm GT}^{\rm exp}(E_x)$ vs E for the indicated nuclei.

pected as a result of mixing of $0\hbar\omega$ GT states with two-particle–two-hole excitations. In addition, $2\hbar\omega$ transitions with $\Delta L = 0$ may be excited. Thus there should be some high-lying $\Delta L = 0$ strength, but the total uncertainty in the quantitative estimates of this analysis is considerably greater than indicated in Fig. 9.

The measured cross sections shown in Fig. 9 have been extrapolated to zero momentum transfer. This extrapolation [Eq. (5)] is a slowly increasing function of Q value below 8.5 MeV of excitation (increasing about 1%/MeV), and was determined for each Ni isotope over the range in excitation energy of the data with the code DW81 [20]. These extrapolated cross sections were then converted to GT strengths using $\hat{\sigma} = 4.49$ for ^{60}Ni, 4.29 for ^{62}Ni, and 4.08 for ^{64}Ni, as determined by measured values of $\hat{\sigma}$ fitted to Eq. (1). We can use our measured unit cross section for the "g.s." peak for ^{64}Ni, together with the global value of $\hat{\sigma}$, to estimate the possible excited-state contribution. The result is $\sigma(\text{exc}) = 23\% \pm 10\%$ of our "g.s." peak, where we have included an estimated 10% uncertainty in the global determination of $\hat{\sigma}$. This value of σ(exc) is consistent with the value from the Q(g.s.) analysis.

The experimental running sums, $\sum_{Ex=0}^{E} B_{\rm GT}^{\rm exp}(E_x)$, are plotted in Fig. 10 for the full range in excitation energy of this experiment (0–30 MeV). As noted earlier, the measured cross sections and consequently estimates of GT strength were subject to large systematic uncertainties above about 8 MeV excitation energy. Because of this, a model comparison, to be discussed below, was restricted to data in the range of excitation energies up to 8.5 MeV, the upper edge of the data in the 8 MeV bin. These total strengths are 3.11 ± 0.08 units for ^{60}Ni, 2.53 ± 0.07 units for ^{62}Ni, and 1.72 ± 0.09 units for ^{64}Ni, where errors are statistical only.

Experimental distributions of GT strength have been

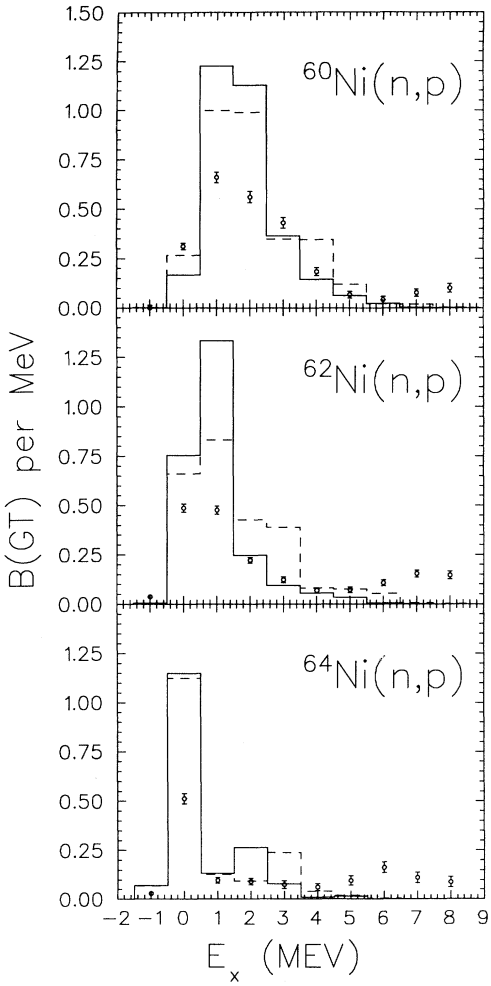

FIG. 12. Experimental GT strength distributions below 8.5 MeV for ^{60,62,64}Ni(n,p) compared with theoretical predictions from the shell model. Calculations employing the FPC8 interaction (solid) and for the FPVH interaction (dashed) have been broadened to match the experimental resolution. Theoretical strengths have been renormalized by factors equal to those in the last two columns of Table II.

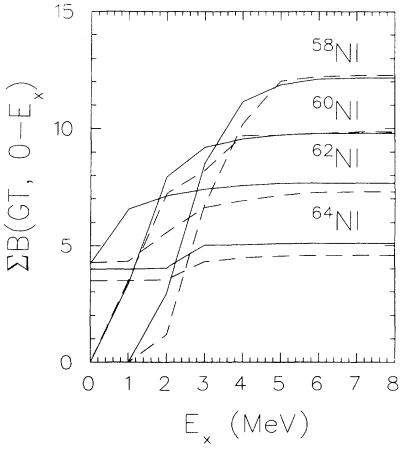

FIG. 11. Theoretical running B(GT) sums for the FPC8 interaction (solid) and for the FPVH interaction (dashed) for the Ni nuclei shown.

TABLE II. Experimental and calculated sums of B_{GT} strength.

Target	Experimental		Shell model (0–8 MeV)		Exp/Th (0–8 MeV)	
	0–8 MeV	0–30 MeV[a]	FPC8	FPVH	FPC8	FPVH
^{58}Ni	3.8 ± 0.4[b]		12.171	12.281	0.312	0.309
^{60}Ni	3.11 ± 0.08[c]	7.4 ± 0.5	9.795	9.859	0.318	0.315
^{62}Ni	2.53 ± 0.07[c]	6.3 ± 0.5	7.671	7.294	0.330	0.347
^{64}Ni	1.72 ± 0.09[c]	4.1 ± 0.9	5.101	4.569	0.337	0.376

[a]Quoted uncertainties are statistical only. Systematic uncertainties may be quite large.
[b]From [25]. Includes a statistical uncertainty of 0.12 and a systematic uncertainty in $\hat{\sigma}$ of 0.38.
[c]Quoted uncertainties are statistical only.

compared with results of shell-model calculations carried out using the code OXBASH [30]. For these calculations a truncated vector space was used with initial state $(f_{7/2})^{16}(f_{5/2}p_{3/2}p_{1/2})^{4,6,8}$ and final state $(f_{7/2})^{15}(f_{5/2}p_{3/2}p_{1/2})^{5,7,9}$ for ^{60}Ni, ^{62}Ni, and ^{64}Ni, respectively. Two effective interactions were used in the calculation. The first (FPC8) was obtained by fitting a large number of binding energies and excitation energies for nuclei in the mass range $41 \leq A \leq 66$ [31]. The second calculation used the FPVH interaction [32]. Theoretical running sums, $\sum_{Ex=0}^{E} B_{GT}(E_x)$, for both interactions and for the nuclei ^{58,60,62,64}Ni are presented as curves in Fig. 11. Both calculations predict a strong concentration of GT strength at low excitations, i.e., prominant peaks of GT strength as are observed experimentally. No significant strength is predicted above 5 MeV excitation, evident as a saturation in the running sums which occurs in about 1.5 MeV intervals with decreasing A. By contrast, Fig. 10 shows that the experimental GT running sums do not saturate in this manner, but increase smoothly to high excitation energy.

For comparison with the data, calculated strengths were broadened to match the experimental resolution and renormalized to the sum to 8.5 MeV excitation of measured strengths. These renormalized results are shown in Fig. 12 for both effective interactions used in the calculations. A summary of measured strengths and renormalization factors is shown in Table II. The agreement between theory and experiment in the general distribution of GT strength with excitation energy is fair for the strong, low-lying GT peaks. However, it is clear that the calculations predict a total strength three to four times greater than is measured at low excitation energies while they fail to account for strength at excitation energies above 8 MeV. It should be noted here that similar calculations employing an expanded vector space [33] showed some spreading of strength to higher excitation and an overall decrease in total strength. The main features of the resulting distributions were similar to those obtained with the more restricted vector space, however.

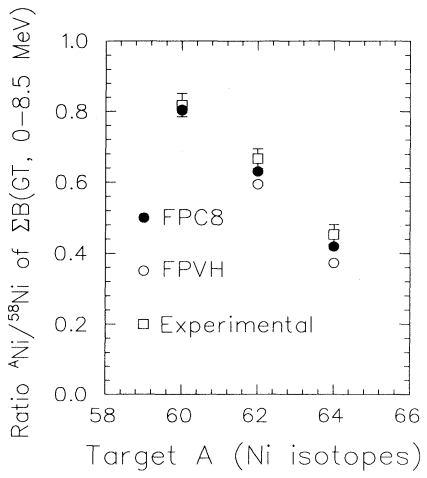

FIG. 13. Ratios of the sum of GT strength up to 8.5 MeV for Ni isotopes A =60, 62, and 64 to the sum for ^{58}Ni. Shown are both shell-model predictions and data derived from the multipole decomposition.

Figure 13 plots vs A the running-sum ratios $\sum_{Ex=0}^{Ex=8.5\ \mathrm{MeV}} B(A)_{GT} / \sum_{Ex=0}^{Ex=8.5\ \mathrm{MeV}} B(A=58)_{GT}$ for the two interactions. Experimental values of this ratio are also given. In the simple shell-model space used here, in which both the $0f_{7/2}$ neutron and proton orbitals are fully occupied, there is an *exact* relationship between the summed GT strength and the $0f_{5/2}$ neutron vacancy in the target. Because all GT transitions are then of the type $\pi 0f_{7/2} \rightarrow \nu 0f_{5/2}$ the two are simply proportional to one another. In ^{58}Ni, with most shell-model interactions, the $0f_{5/2}$ neutron vacancy is about 5.7 (out of a maximum of 6), and for other even Ni isotopes, it decreases reasonably smoothly. In Fig. 13, we note that the experimental and theoretical ratios behave similarly. We repeat that the relationship is exact for the shell-model results.

Koonin and Langanke [34] have suggested that, for even-Z nuclei, the sum of GT strength to 8.5 MeV is proportional to the product of the numbers of valence protons and *total* fp neutron holes for mid-fp-shell nuclei. They state that they expect their relationship to be valid for nuclei from ^{48}Ti to ^{70}Ge, i.e., for $22 \leq Z \leq 32$ and $26 \leq N \leq 38$. We would be very surprised if this conjecture were true. We note that for our present Ni results, their expression gives a total χ^2 that is 3.4 times as large as the assumption of uniform quenching. More, and better, experiments should be able to test their hypothesis. Their conjecture might hold better in the $0f_{5/2}$, $1p_{3/2}$, $1p_{1/2}$ subspace, if generalized seniority is a good approximation.

Whereas the distribution of GT strength to 8.5 MeV calculated with the FPC8 interaction agrees well with

experiment for the nearby nuclei ^{54}Fe, ^{55}Mn, and ^{56}Fe, it has been shown that the disagreement is large for ^{58}Ni [25]. This result is quite sensitive to the details of the single-particle Hamiltonian [34]. Table II illustrates that the quenching factor is roughly constant down the Ni isotopic chain.

IV. CONCLUSIONS

We have measured differential cross sections for the (n,p) reaction on ^{60,62,64}Ni at 198 MeV in order to determine Gamow-Teller strength distributions as a function of excitation energy. The cross section per unit GT strength, $\hat{\sigma}_{\rm GT}$, was estimated for the nucleus ^{64}Ni, subject to the possibility that a low-lying 1^+ state may contribute to the measured cross section. If the excited state is not populated, we have $\hat{\sigma} = 5.3 \pm 0.4$ mb/sr. If its strength is 40% $\pm$ 16% of the g.s., then $\hat{\sigma} = 3.2 \pm 0.9$. A better determination of $\hat{\sigma}$ would require measurements with superior energy resolution than could be achieved in the present experiment.

The measured GT strength distributions have been compared with shell-model calculations. Predicted strength distributions are too large overall by a factor of about 3 but reproduce the basic trend of measured GT strength below 6 MeV. At very low excitation energies and above about 6 MeV, the renormalized calculations underestimate the data. Model comparisons of this sort are useful to assess the confidence which may be placed on predictions for GT strength in cases which may not be determined by measurement.

ACKNOWLEDGMENTS

This work was supported by grants from the Natural Sciences and Engineering Research Council of Canada and from the U. S. National Science Foundation.

[1] T. N. Taddeucci, C. A. Goulding, T. A. Carey, R. C. Byrd, C. D. Goodman, C. Gaarde, J. Larsen, D. Horen, J. Rapaport, and E. Sugarbaker, Nucl. Phys. **A469**, 125 (1987).
[2] W. P. Alford, R. L. Helmer, R. Abegg, A. Celler, O. Häusser, K. Hicks, K. P. Jackson, C. A. Miller, S. Yen, R. E. Azuma, D. Frekers, R. S. Henderson, H. Baer, and C. D. Zafiratos, Phys. Lett. B **179**, 20 (1986).
[3] S. E. Woosley, W. D. Arnett, and D. D. Clayton, Astrophys. J. **175**, 731 (1972).
[4] G. M. Fuller, W. A. Fowler, and M. J. Newman, Astrophys. J. **252**, 715 (1982).
[5] J. Cooperstein and J. Wambach, Nucl. Phys. **A420**, 591 (1984).
[6] M. B. Aufderheide, Nucl. Phys. **A526**, 161 (1991).
[7] M. B. Aufderheide, G. E. Brown, T. T. S. Kuo, D. B. Stout, and P. Vogel, Astrophys. J. **362**, 241 (1990).
[8] O. Hausser *et al.*, unpublished.
[9] M. L. Halbert, Nucl. Data Sheets **28**, 179 (1979); B. Singh, *ibid.* **62**, 603 (1991).
[10] V. Rahkonen and J. Kantele, Phys. Fenn. **9**, 103 (1974).
[11] D. H. Wilkinson, Nucl. Phys. **A377**, 474 (1982).
[12] A. Bohr and B. M. Mottelson, *Nuclear Structure* (Benjamin, New York, 1969), Vol. I, p. 411.
[13] R. Helmer, Can. J. Phys. **65**, 588 (1987).
[14] R. S. Henderson, W. P. Alford, D. Frekers, O. Häusser, R. L. Helmer, K. H. Hicks, K. P. Jackson, C. A. Miller, M. C. Vetterli, and S. Yen, Nucl. Instrum. Methods Phys. Res. Sect. A **257**, 97 (1987).
[15] R. A. Arndt and L. D. Roper, Scattering Analysis Interaction Dial-in (SAID) program (SM90), unpublished; R. A. Arndt *et al.*, Phys. Rev. D **45**, 3995 (1992).
[16] E. R. Flynn and J. D. Garrett, Phys. Lett. **42B**, 49 (1972).
[17] E. Runte, K.-L. Gippert, W.-D. Schmidt-ott, P. Tidemand-Petersson, L. Ziegeler, P. Kerchner, O. Klepper, P. O. Larsson, E. Roeckl, D. Schardt, N. Kaffrell, P. Peuser, M. Bernas, P. Dessagne, M. Langevin, and K. Rykaczewski, Nucl. Phys. **A441**, 237 (1985).
[18] M. S. Antony, J. Britz, and A. Pape, At. Data Nucl. Data Tables **40**, 9 (1988).
[19] M. Marty, C. Djalali, M. Morlet, A. Willis, J. C. Jourdain, N. Anantaraman, G. M. Crawley, and A. Galonsky, Nucl. Phys. **A396**, 145c (1983).
[20] R. Schaeffer and J. Raynal, computer code DWBA70, Arizona State University, 1970 unpublished; extended version: J. R. Comfort, computer code DW81, Arizona State University, 1984, unpublished.
[21] M. A. Franey and W. G. Love, Phys. Rev. C **31**, 488 (1985).
[22] Computer code MAINX8, T. Cooper, private communication; modified by R. G. Jeppesen, unpublished.
[23] M. C. Vetterli, O. Häusser, R. Abegg, W. P. Alford, A. Celler, D. Frekers, R. Helmer, R. Henderson, K. Hicks, K. P. Jackson, R. G. Jeppesen, C. A. Miller, K. Raywood, and S. Yen, Phys. Rev. C **40**, 559 (1989).
[24] W. P. Alford, B. A. Brown, S. Burzynski, A. Celler, D. Frekers, R. Helmer, R. Henderson, K. P. Jackson, K. Lee, A. Rahav, A. Trudel, and M. C. Vetterli, Phys. Rev. C **48**, 2818 (1993).
[25] S. El-Kateb, K. P. Jackson, W. P. A. Alford, R. Abegg, R. E. Azuma, B. A. Brown, A. Celler, D. Frekers, O. Hausser, R. Helmer, R. S. Henderson, K. H. Hicks, R. Jeppesen, J. D. King, K. Raywood, G. G. Shute, B. M. Spicer, A. Trudel, M. Vetterli, and S. Yen, Phys. Rev. C **49**, 3129 (1994).
[26] A. Ling, X. Aslanoglou, F. P. Brady, R. W. Finlay, R. C. Haight, C. R. Howell, N. S. P. King, P. W. Lisowski, B. K. Park, J. Rapaport, J. L. Romero, D. S. Sorenson, W. Tornow, and J. L. Ullmann, Phys. Rev. C **44**, 2794 (1991).
[27] M. A. Moinester, Can. J. Phys. **65**, 660 (1987).
[28] A. Klein and N. Auerbach, Phys. Rev. C **30**, 1032 (1984).
[29] D. J. Mercer, J. Rapaport, C. A. Whitten, Jr., D. Adams,

R. Byrd, X. Y. Chen, A. Fazely, T. Gaussiran, E. Gulmez, C. Goodman, D. W. Huang, G. Igo, A. Ling, D. Marchlenski, D. Prout, L. Rybarcyk, D. Sugarbaker, and T. N. Taddeucci, Phys. Rev. C **49**, 3104 (1994).

[30] B. A. Brown, A. Etchegoyen, W. D. M. Rae, and N. S. Godwin, The Oxford-Buenos Aires-MSU shell model code (OXBASH) MSUCL Report No. 524, 1986, unpublished.

[31] W. A. Richter, M. G. Van Der Merwe, R. E. Julies, and B. A. Brown, Nucl. Phys. **A523**, 325 (1991).

[32] J. F. A. Van Hienen, W. Chung, and B. H. Wildenthal, Nucl. Phys. **A269**, 159 (1976).

[33] M. B. Aufderheide, S. D. Bloom, D. A. Resler, and G. J. Mathews, Phys. Rev. C **47**, 2961 (1993).

[34] S. E. Koonin and K. Langanke, Phys. Lett. B **326**, 5 (1994).